

Multiple Contexts and Frequencies Aggregation Network for Deepfake Detection

Zifeng Li
Beihang University
lizifeng@buaa.edu.cn

Wenzhong Tang
Beihang University
tangwenzhong@buaa.edu.cn

Shijun Gao
Beihang University
gaoshijun@buaa.edu.cn

Shuai Wang
Beihang University
wangshuai@buaa.edu.cn

Yanxiang Wang*
Beihang University
wangyanyang@buaa.edu.cn *

Abstract

Deepfake detection faces increasing challenges since the fast growth of generative models in developing massive and diverse Deepfake technologies. Recent advances rely on introducing heuristic features from spatial or frequency domains rather than modeling general forgery features within backbones. To address this issue, we turn to the backbone design with two intuitive priors from spatial and frequency detectors, i.e., learning robust spatial attributes and frequency distributions that are discriminative for real and fake samples. To this end, we propose an efficient network for face forgery detection named MkfaNet, which consists of two core modules. For spatial contexts, we design a Multi-Kernel Aggregator that adaptively selects organ features extracted by multiple convolutions for modeling subtle facial differences between real and fake faces. For the frequency components, we propose a Multi-Frequency Aggregator to process different bands of frequency components by adaptively reweighing high-frequency and low-frequency features. Comprehensive experiments on seven popular deepfake detection benchmarks demonstrate that our proposed MkfaNet variants achieve superior performances in both within-domain and across-domain evaluations with impressive efficiency of parameter usage.

1. Introduction

With the development of generative models, Deepfake technology has made significant progress. Deepfake encompasses video, audio, and text, utilizing advanced artificial intelligence techniques such as Variational Autoencoders (VAE) [32], Generative Adversarial Networks (GAN) [10], and Diffusion Models (DM) [11] to achieve

*Yanxiang Wang is the corresponding author.

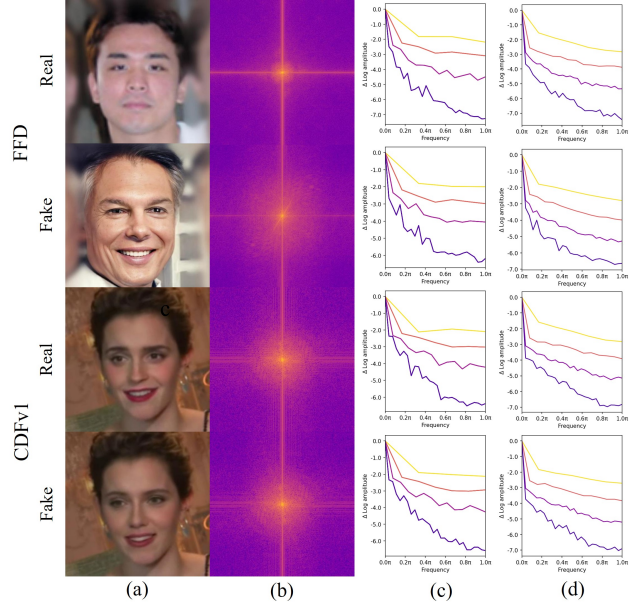


Figure 1. Illustration of frequency priors in deepfake detection. (a): Source image. (b): Data frequency domain analysis. (c): Relative log amplitudes of Fourier transformed feature maps of ResNet50. (d): Relative log amplitudes of Fourier transformed feature maps of MkfaNet. (b) reveals the uniformity of the frequency distribution in real faces and the concentration of high-frequency anomalies in forged faces. (c) shows that ResNet50 has a relatively low logarithmic amplitude in the high-frequency region, indicating its insufficiency in capturing high-frequency details. (d) demonstrates that MkfaNet has a higher amplitude in the high-frequency region with broader coverage, highlighting its advantages in handling high-frequency details and identifying forgery features.

unprecedented realism. Unfortunately, these fake visual data can be used for malicious purposes, such as invading personal privacy, spreading misinformation, and undermining people’s trust in digital media [3, 61]. Considering that

facial deepfakes can potentially cause more significant social and ethical implications compared to synthetic media without facial content, we specifically concentrate on facial deepfake technology in this paper.

To address the potential risks posed by Deepfakes, numerous researchers are working to enhance Deepfake detection technology and strengthen existing detection systems [2, 20–22, 35]. These methods employ various techniques and are generally classified into three types: naive detectors [1, 52], spatial detectors [4, 62], and frequency detectors [45, 51]. Meanwhile, researchers are striving to develop sufficiently robust detectors to withstand various forms of degradation, such as noise [25, 28, 38], compression [35, 66], and, most critically, to identify previously unseen Deepfakes [50, 55]. Therefore, enhancing the generalization ability of Deepfake detection models becomes particularly important. Models with strong generalization capabilities can effectively identify and counter new Deepfake attacks that have not appeared in the training data, thereby ensuring the authenticity and security of information [34].

Improving the model’s ability to capture critical facial features is an effective means of enhancing its generalization capability. These key features include but are not limited to, subtle dynamics of facial expressions, natural gradients of skin tone, and natural eye blinking. By accurately capturing these difficult-to-simulate details, the model can more effectively distinguish between real content and Deepfake-generated content [25]. In recent research, adopting multitask learning [5, 6, 37, 71] and/or heuristic fake data generation strategies [37, 54] is the mainstream method to enhance the generalization capability of Deepfake detection method. These approaches aim to improve the model’s adaptability and discrimination ability against novel forgery techniques by learning multiple related tasks simultaneously. Meanwhile, heuristic data generation methods create new and unseen fake samples to test and improve the robustness of detection algorithms. However, commonly used architectures for these methods, such as XceptionNet [9] and EfficientNet [57], primarily tend to learn global features while neglecting more local features [64, 70, 73]. Consequently, most of these methods fail to effectively model local artifacts, which is crucial for detecting high-quality Deepfake content.

We first focus on the differences between real and forged samples in the frequency domain, and our empirical analysis reveals significant disparities in their frequency distributions, as shown in Figure 1(b). Specifically, real samples exhibit a relatively uniform energy distribution in the spectrogram, indicating a balanced texture and edge information across various frequencies. In contrast, forged samples display abnormally concentrated energy peaks in the high-frequency region, highlighting the shortcomings of forgery techniques in handling high-frequency details, which result

in unnatural textures and edges in the high-frequency area. To further illustrate this phenomenon, we use a pre-trained ResNet50 model to examine how it processes real and fake face images, with the results shown in Figure 1(c). Notably, ResNet50 exhibits a weaker response in the high-frequency region, indicating its insufficiency in capturing the high-frequency details of forged faces. Additionally, when processing forged face images, ResNet50’s shallow feature maps exhibit higher low-frequency responses, whereas these low-frequency responses are weaker and more uniformly distributed when processing real faces. This indicates that ResNet50 has a stronger reaction to simple features in forged images but lacks sensitivity to high-frequency details. This layered difference in frequency response reveals the underlying mechanisms by which deep networks distinguish between real and fake faces. It provides important insights and motivation for designing models that can more accurately differentiate between genuine and forged faces.

Additionally, we have observed that recent advances rely on introducing heuristic features from either the spatial or frequency domain, rather than establishing a general forgery feature detection model within the backbone network. While this approach improves detection performance to some extent, it still has limitations, especially in addressing the continuously evolving forgery techniques. Therefore, we propose MkfaNet, which integrates more powerful feature capture and analysis capabilities into the backbone network by combining the Multi-Kernel Aggregator (MKA) and Multi-Frequency Aggregator (MFA), significantly enhancing the accuracy and robustness of forgery detection. In specific, the Multi-Kernel Aggregator (MKA) module combines depth-wise separable convolutions with different dilation rates to effectively expand the model’s receptive field, enhancing its ability to capture features at various scales from the input data. It then adaptively selects features extracted through multiple convolutions based on the spatial context to model the subtle facial differences between real and fake faces; Multi-Frequency Aggregator (MFA) module optimizes the model’s response to different frequency information by separately processing and fusing the DC (Direct Current) and HC (High Current) components of images. MkfaNet, as a stack of MKA and MFA modules, shows the enhanced ability to discern image details and structural information. In the context of real and fake face recognition, it can accurately distinguish the subtle texture and frequency distortions introduced by forgery techniques, thereby improving the accuracy of fake image detection.

Comprehensive experiments on seven popular deepfake detection benchmarks [68] demonstrate that our proposed MkfaNet variants achieve superior performances in both within-domain and across-domain evaluations with impressive efficiency of parameter usage.

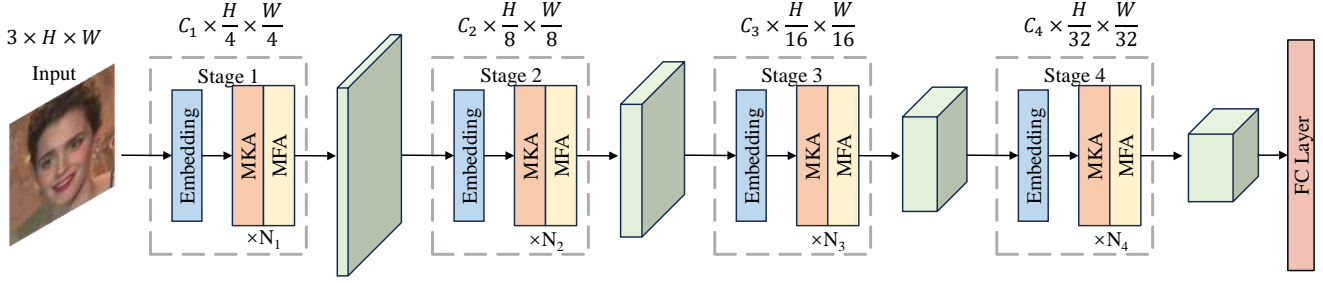


Figure 2. MkfaNet architecture with four stages. MkfaNet uses a hierarchical architecture of 4 stages. Each stage i consists of an embedding stem, N_i Multi-Kernel Aggregator (MKA), and Multi-Frequency Aggregator (MFA) Blocks.

2. Related Work

Deepfake Generation Deepfake technology primarily involves the artificial modification of facial images and has significantly evolved since its inception. Since 2017, machine learning-based facial manipulation techniques have made substantial advancements, particularly in the areas of facial replacement and facial expression reenactment, which have garnered widespread attention [68]. Ian Goodfellow et al. introduced Generative Adversarial Networks (GANs) [24], a technology that has significantly advanced the development of realistic image synthesis, including facial images [8, 29]. GANs consist of two parts: the generator and the discriminator. The generator is responsible for creating images, while the discriminator’s task is to distinguish between these generated images and real data. Variational Autoencoders (VAEs) [31] compress data into a compact form and are used in Deepfake technology to alter facial features, such as expressions and styles. Diffusion models (DMs) [23, 72] create images by gradually adding noise and then progressively removing this noise during the generation process. In facial image generation, diffusion models can produce high-quality, high-resolution facial images by finely controlling the noise reduction process. Facial Deepfakes can be broadly categorized into two types: face-swapping and face-reenactment. Face-swapping refers to replacing the facial features in one image with the facial features from another image [36, 48, 49]. Face-reenactment technology modifies the original face using image processing techniques to mimic the expressions of another face. Face2Face [59] generates different expressions by tracking facial key points, while NeuralTextures [58] achieves expression transfer using rendered images generated from 3D facial models. These technologies enable more diverse and precise simulation of facial expressions.

Deepfake Detection In Deepfake detection research, there are two main types: image-level detectors and video-level detectors. Image-level detectors identify fake images by recognizing spatial artifacts in single frames. A direct method for detecting spatial artifacts is using the Xception model [52], a convolutional neural network (CNN)

architecture, combined with the use of attention mechanisms like MAT [70]. Face X-ray [37] proposed a method that uses boundaries between forged faces and backgrounds to capture spatial inconsistency. Recently, algorithms utilize methods including blending artifacts [2, 18] or separating elements relevant to detection from irrelevant ones during their training. In contrast to image-level detectors, video-level detectors take advantage of temporal information by using multiple frames to detect deepfake videos [7]. Recently, FTCN [74] directly extracted temporal information using 3D CNNs with a spatial kernel size of 1. AlFreeze [65] showcases strong generalization capabilities through its unique approach of independently training spatial and temporal information. Despite their great potential, the aforementioned models are less robust when considering high-quality deepfakes. Indeed, these SoA methods mainly employ traditional DNN backbones such as XceptionNet [9] and EfficientNet [57].

Therefore, these network models implicitly form global features through their successive convolutional layers. This can lead to some critical and useful features being unintentionally overlooked, thereby affecting the effective detection of high-quality Deepfake content. Thus, it is essential to develop effective strategies that focus on capturing key features to achieve high-quality and effective detection.

3. Method

3.1. Overview of MkfaNet

Built upon modern ConvNets, we design a four-stage MkfaNet architecture as illustrated in Figure 2. For stage i , the input image or feature is first fed into an embedding stem to regulate the resolutions and embed into C_i dimensions. Assuming the input image in $H \times W$ resolutions, features of the four stages are in $\frac{H}{4} \times \frac{W}{4}$, $\frac{H}{8} \times \frac{W}{8}$, $\frac{H}{16} \times \frac{W}{16}$, and $\frac{H}{32} \times \frac{W}{32}$ resolutions respectively. Then, the embedded feature flows into N_i Mkfa Blocks, consisting of spatial and channel aggregation blocks, for multi-kernel feature and high-low frequency aggregation.

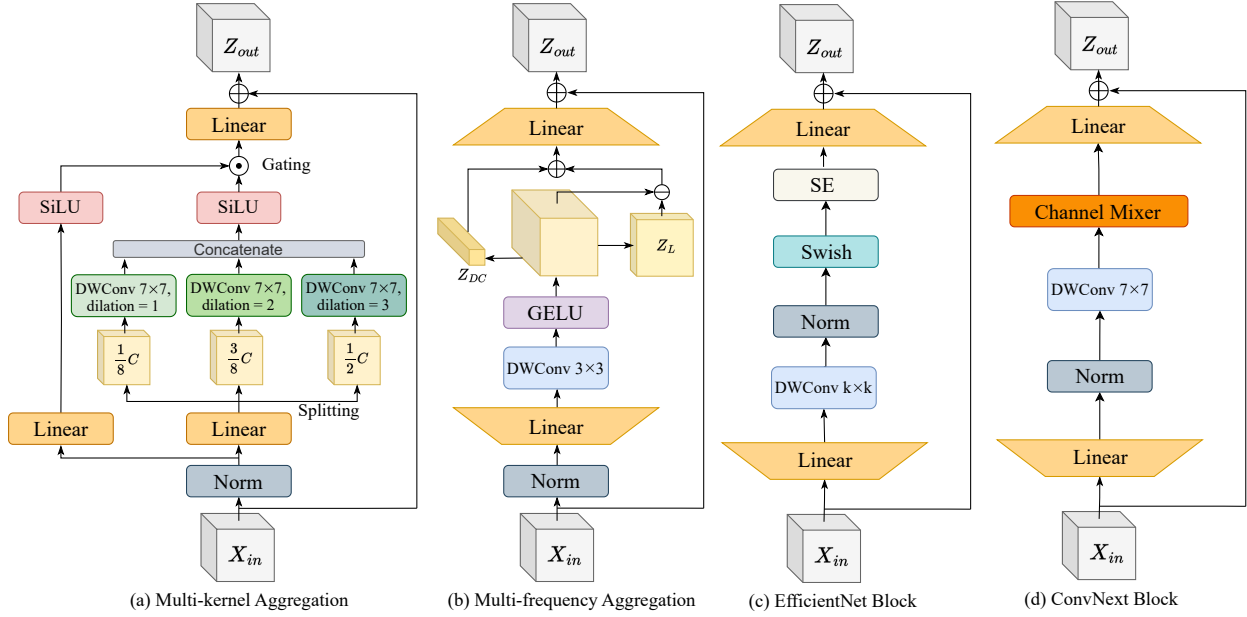


Figure 3. (a) Structure of multi-kernel aggregation block as token mixer. (b) Structure of multi-frequency aggregation block as the channel mixer. (c) The basic building block of the EfficientNet model. (d) Structure of ConvNext block.

3.2. Multi-kernel Aggregator

Model generative models are able to create extremely realistic fake human faces that are visually almost indistinguishable from real ones by learning from a vast amount of real facial data and thus simulating features such as lighting, texture, and shape of faces. In this context, traditional single-scale feature extraction methods struggle to detect these fake faces. This is mainly because such methods typically focus on features at a fixed scale, such as coarse patterns of edges or textures, and overlook the subtle changes and complex interactions across multiple scales, which are precisely what generation techniques excel at simulating.

Therefore, to effectively distinguish these high-quality fake images from real faces, a method capable of analyzing and identifying details at multiple levels is required. In this way, we propose MKA modules as a solution, which adaptively selects organ features extracted by multiple convolutions for modeling subtle facial differences between real and fake faces. To elucidate the implementation details of the Multi-kernel Aggregator (MKA) module, as illustrated in Figure 3(a), we will delve into its architectural design, focusing on how it adaptively aggregates multi-level features to enhance the detection of key facial regions. We represent this process as follows:

$$Z = X + \text{MKA}(\text{Norm}(X)), \quad (1)$$

where $\text{MKA}(\cdot)$ denotes a multi-kernel gated aggregation module comprising the gating $\mathcal{F}_\phi(\cdot)$ and multi-kernel feature branch $\mathcal{G}_\psi(\cdot)$.

Multi-kernel feature extraction. To enable the model to perceive the multi-level features of the face images, we employ three different DWConv layers with dilation ratios $d \in \{1, 2, 3\}$ in parallel to capture low, middle, and high-order features: given the input feature $X \in \mathbb{R}^{C \times HW}$, the input is factorized into $X_l \in \mathbb{R}^{C_l \times HW}$, $X_m \in \mathbb{R}^{C_m \times HW}$, and $X_h \in \mathbb{R}^{C_h \times HW}$ along the channel dimension, where $C_l + C_m + C_h = C$; afterward, X_l , X_m and X_h are assigned to $\text{DW}_{7 \times 7, d=1}$, $\text{DW}_{7 \times 7, d=2}$ and $\text{DW}_{7 \times 7, d=3}$, respectively. Finally, the output of X_l , X_m , and X_h are concatenated to form multi-kernel feature, so that $Y_C = \text{Concat}(Y_l, Y_m, Y_h)$.

Gated Aggregation. To *adaptively* aggregate the extracted feature from the multi-kernel feature branch, and we employ SiLU activation in the gating branch, as $\text{SiLU}(x) = x \cdot \text{Sigmoid}(x)$, which has been well-acknowledged as an advanced version of Sigmoid activation. SiLU has both the gating effect of Sigmoid and stable training characteristics, leading the final aggregated features as

$$Z = \underbrace{\text{SiLU}(\text{Conv}_{1 \times 1}(X))}_{\mathcal{F}_\phi} \odot \underbrace{\text{SiLU}(\text{Conv}_{1 \times 1}(Y_C))}_{\mathcal{G}_\psi}. \quad (2)$$

3.3. Multi-Frequency Aggregator

Fig 1(b) shows the frequency domain analysis of the data, revealing significant differences in the distribution of high-frequency information between fake and real faces. Fake faces often appear unnatural in details such as skin

texture and edge sharpness, resulting in a noticeably different distribution of features in the high-frequency region. Fig 1(c) illustrates the relative logarithmic amplitude of the Fourier-transformed data, with the color gradient from purple to yellow representing the transition from shallow to deep layers of the model. This gradient reveals how layers of different depths handle frequency information, providing visual evidence of the differences in frequency responses between real and fake faces.

It is evident that the shallow layers (purple) tend to capture high-frequency details related to texture and edges, while the deeper layers (yellow) strongly respond to low-frequency features, which are typically associated with the overall structure and shape of the image. At these levels, real and fake faces exhibit different frequency characteristics. Specifically, in the high-frequency details, fake faces often fail to perfectly replicate the high-frequency features of real faces due to technical limitations, resulting in anomalies or inconsistencies in the high-frequency region. This underscores the importance of addressing both low-frequency and high-frequency features in facial recognition.

We propose an MFA module that processes and reorganizes the direct current (DC) and high-frequency (HC) components of images independently, allowing the model to perform more refined and in-depth analysis at different frequency levels. Specifically, the MFA enhances the analysis of high-frequency details to identify unnatural textures and edges produced by generative models while integrating low-frequency information to maintain an understanding of the overall structure of the image. This approach not only strengthens the model’s ability to detect flaws unique to forgery techniques but also improves its capacity to capture authentic features. As a result, the accuracy and robustness of facial authenticity recognition are significantly enhanced. By comprehensively analyzing features at different frequencies, the MFA helps the model better distinguish and recognize complex real and fake faces, effectively addressing the challenges posed by high-quality forgery techniques. The structure of the MFA module, as shown in Figure 3(b), can be formalized as follows:

$$\begin{aligned} Y &= \text{GELU}\left(\text{DW}_{3\times 3}(\text{Conv}_{1\times 1}(\text{Norm}(X)))\right), \\ Z &= \text{Conv}_{1\times 1}(\text{MF}(Y)) + X. \end{aligned} \quad (3)$$

where $\text{MF}(\cdot)$ is a scaling technique that operates on feature maps by distinctively mixing information from different frequency bands. In specific, the input signal is firstly decomposed into its DC component and high-frequency components. Then, two sets of parameters are introduced to re-weight these components for each channel. The two-step

processing reads as,

$$\begin{aligned} Y_{DC} &= z_{DC} \odot Y, \\ Y_{HC} &= Y - z_L \odot Y, \\ \text{MF}(Y) &= Y_{DC} + \gamma \odot Y_{HC}, \end{aligned} \quad (4)$$

where γ is the channel-wise scaling factor initialized as zeros. The calculation of DC and HC components is also computationally efficient, as it does not require explicit Fourier transforms. The DC component is calculated by averaging each feature map, while the HC component is obtained by subtracting the DC component from the original features. Specifically, z_{DC} represents the spatial average, and z_L represents the channel average.

3.4. Discussion

3.4.1 Advantages over Classical CNN

Currently, the commonly used architectures for fake face detection are XceptionNet [9] and EfficientNet [57], which primarily focus on learning global features [64, 70]. The XceptionNet architecture uses depthwise separable convolution layers to build its structure. This design optimizes the learning of global features, making the model excel in recognizing overall structures and patterns in images. However, in tasks like fake face detection, which require fine analysis of local details, this tendency may limit the model’s sensitivity to subtle facial expression differences and skin texture patterns.

EfficientNet is an optimized convolutional neural network architecture that enhances model efficiency and feature representation by balancing adjustments to network depth, width, and resolution and integrating depthwise separable convolutions and Squeeze-and-Excitation (SE) blocks. Its architecture is illustrated in Figure 3(a). Although SE blocks improve the model’s attention to features, this re-calibration is based on global information and cannot capture the specific local detail anomalies characteristic of forged faces. The performance gain of EfficientNet is attributed to its adjusting resolution. However, in fake face detection, sensitivity to subtle local feature variations is crucial. Simply relying on resolution adjustments is inadequate to counter high-quality face forgery techniques [14].

Although Xception and EfficientNet employ innovative optimizations, adhering to traditional CNN design principles introduces certain disadvantages. Hierarchical feature extraction may not fully capture the global context and long-range dependencies in images, limiting their ability to handle complex data. Additionally, increasing the number of layers and network width enhances performance but significantly raises the model’s parameter count and computational cost.

3.4.2 Advantages over Modern DNN

The design of modern deep neural networks (DNNs) offers significant advantages, including higher representational capacity and computational efficiency. By employing block-based designs combined with hierarchical and isotropic stages, they can effectively handle large-scale and complex datasets, capture long-range dependencies, and perform multi-scale feature extraction. Additionally, these networks can adaptively adjust the functionality and dimensions of each layer, providing greater flexibility to meet different task requirements, thereby significantly improving model performance while maintaining parameter efficiency.

ConvNext [43] is a modern convolutional neural network architecture. Figure 3(b) shows the architecture of its basic module. By using a channel mixer, ConvNext enhances the use of inter-channel information by mixing features from different channels, thus enriching feature representation. While the channel mixer improves the interaction between different channels, it may still lack sensitivity to local detail features, especially the subtle anomalies in forged faces. Therefore, although this model performs well in general image tasks, it may require further adjustments or integration with other mechanisms for specialized fake face detection tasks to better capture and analyze the inherent local and high-frequency detail features of forgery techniques.

Based on the above analysis and addressing the issues in commonly used architectures for fake face detection, we have constructed a unique architecture specifically for this task. This architecture is designed with modern deep neural network (DNN) principles in mind and incorporates multi-kernel feature adaptive fusion modules (MKA) and multi-frequency adaptive fusion modules (MFA), as shown in Fig 3(c) and (d), respectively. The MKA module targets spatial context by adaptively selecting organ-specific features extracted through multiple convolutions to simulate the subtle facial differences between real and fake faces. The MFA module focuses on frequency components, processing different frequency bands by adaptively rebalancing high-frequency and low-frequency features.

4. Experiments

4.1. Settings

Datasets. To evaluate the performances and generalization abilities of our proposed backbone, we follow DeepfakeBench [68] to conduct comparison and analysis experiments on seven commonly used deepfake detection datasets: FaceForensics++ (FF++) [52], CelebDF-v1 (CDFv1) [40], CelebDF-v2 (CDFv2) [40], DeepFakeDetection (DFD) [15], DeepFake Detection Challenge Preview (DFDC-P) [17], DeepFake Detection Challenge (DFDC) [16], and DeeperForensics-1.0 (DF-1.0) [28]. Specifically, FF++ is a large-scale database with 1.8 mil-

lion forged images that contains 4 types of manipulation methods, including Deepfakes (FF-DF) [13], Face2Face (FF-F2F) [59], FaceSwap (FF-FS) [19], and NeuralTextures (FF-NT) [58]. Note that we use the lightly compressed (c23) version of FF++ as the default training data, whereas two other compressed versions of FF++ are raw and heavily compressed (c40), while others are used as testing datasets. We also adopt the full data pre-processing workflow proposed in DeepfakeBench and use the fixed training and testing resolutions of 256×256 for the cropped face images.

Implementation Details. For a fair comparison, we consider three types of detectors in DeepfakeBench, as detailed in Table 1: (1) **Naive detectors** that combine a backbone and binary classifier without introducing manually designed features. Both classical CNNs (*e.g.*, ResNet [26] and EfficientNet [57]) and modern architectures (*e.g.*, Swin Transformer [42] and ConvNeXt [43]) are compared. (2) **Spatial detectors** that build upon the backbone and further utilize spatial features with manual-designed algorithms. (3) **Frequency detectors** focus on exploring frequency components and artifacts to detect forgeries. As for training settings, we train detectors with classical CNNs as the backbone by Adam optimizer [30] with a learning rate of 2×10^{-4} and a batch size of 32 for all experiments. Following ConvNeXt [43], we employ AdamW optimizer [44] to fine-tune detectors with modern backbones using the learning rate of 5×10^{-4} and the batch size of 256. Pre-trained weights of the backbone on ImageNet-1K [33] will be used if feasible, and our MkfaNet adopts the same pre-training setting as ConvNeXt-T [43] on ImageNet-1K. We also apply data augmentations, including image compression, horizontal flip, rotation, Gaussian blur, and random brightness contrast. As for evaluation metrics, we conduct the **frame-level Area Under Curve (AUC)** to compare our proposed MkfaNet with existing works, where the mean result over three trials is reported.

4.2. Comparison Results

As shown in Table 1, we conduct within-domain and cross-domain evaluations for three versions of our MkfaNet, *i.e.*, the lightweight detectors, the naive detectors compared to various backbones, and the advanced detectors with prior knowledge from spatial or frequency domains. cross-domain evaluation involves testing the model on different datasets.

Within-domain Evaluations. We first conduct within-domain evaluations to verify the performances of detectors within the same dataset following DeepfakeBench [68]. Table 1 (middle columns) shows MkfaNet variants achieve the best average results on six within-domain datasets. As for the lightweight detectors, MkfaNet-T significantly outper-

Table 1. Within-domain and cross-domain evaluations of various deepfake detectors and backbones using the AUC metric. All detectors are trained on FF-c23 and evaluated on other datasets. **Avg.** donates the average AUC for within-domain and cross-domain evaluations, and the best result for each group is highlighted in **bold**. † represents our reproduced results, while DeepfakeBench provides others.

Type	Detector	Backbone	# Param. (M)	Within Domain Evaluation							Cross Domain Evaluation						
				FF-c23	FF-c40	FF-DF	FF-F2F	FF-FS	FF-NT	Avg.	CDFv1	CDFv2	DF-1.0	DFD	DFDC	DFDCP	Avg.
Naive	Meso4 [1]	MesoNet	0.03	0.6077	0.5920	0.6771	0.6170	0.5946	0.5701	0.6097	0.7358	0.6091	0.9113	0.5481	0.5560	0.5994	0.6599
Naive	MesoIncep [1]	MesoNet	0.03	0.7583	0.7278	0.8542	0.8087	0.7421	0.6517	0.7571	0.7366	0.6966	0.9233	0.6069	0.6226	0.7561	0.7237
Spatial	Capsule [46]	Capsule	4.0	0.8421	0.7040	0.8669	0.8634	0.8734	0.7804	0.8217	0.7909	0.7472	0.9107	0.6841	0.6465	0.6568	0.7394
Naive	CNN-Aug [63]	ResNet-34	22	0.8493	0.7846	0.9048	0.8788	0.9026	0.7313	0.8419	0.7420	0.7027	0.7993	0.6464	0.6361	0.6170	0.6906
Naive	MkfaNet	MkfaNet-T	5.2	0.8506	0.7879	0.8982	0.8823	0.9037	0.7796	0.8504	0.7881	0.7486	0.9245	0.6883	0.6477	0.7428	0.7567
Naive	CNN-Aug [63]	ResNet-50†	26	0.8925	0.7956	0.9258	0.9135	0.9252	0.7828	0.8726	0.7608	0.7591	0.8143	0.6995	0.6661	0.6245	0.7207
Naive	Xception [52]	Xception	23	0.9637	0.8261	0.9799	0.9785	0.9833	0.9385	0.9450	0.7794	0.7365	0.8341	0.8163	0.7077	0.7374	0.7686
Naive	Efficient [57]	Efficient-B4	19	0.9567	0.8150	0.9757	0.9758	0.9797	0.9308	0.9389	0.7909	0.7487	0.8330	0.8148	0.6955	0.7283	0.7685
Naive	Swin [42]	Swin-T†	28	0.9630	0.8278	0.9802	0.9783	0.9826	0.9375	0.9449	0.7863	0.7476	0.8384	0.8028	0.7053	0.7339	0.7691
Naive	ConvNeXt [43]	ConvNeXt-T†	29	0.9644	0.8287	0.9796	0.9801	0.9840	0.9393	0.9460	0.7837	0.7491	0.8425	0.8102	0.7075	0.7366	0.7716
Naive	MkfaNet	MkfaNet-S	20	0.9671	0.8315	0.9826	0.9820	0.9849	0.9428	0.9485	0.7946	0.7538	0.8785	0.8166	0.7127	0.7413	0.7829
Frequency	F3Net [51]	Xception	23	0.9635	0.8271	0.9793	0.9796	0.9844	0.9354	0.9449	0.7769	0.7352	0.8431	0.7975	0.7021	0.7354	0.7650
Frequency	SPSL [41]	Xception	23	0.9610	0.8174	0.9781	0.9754	0.9829	0.9299	0.9408	0.8150	0.7650	0.8767	0.8122	0.7040	0.7408	0.7856
Frequency	SRM [45]	Xception	23	0.9576	0.8114	0.9733	0.9696	0.9740	0.9295	0.9359	0.7926	0.7552	0.8638	0.8120	0.6995	0.7408	0.7773
Spatial	FWA [39]	Xception	23	0.8765	0.7357	0.9210	0.9000	0.8843	0.8120	0.8549	0.7897	0.6680	0.9334	0.7403	0.6132	0.6375	0.7303
Spatial	X-ray [37]	HRNet	22	0.9592	0.7925	0.9794	0.9872	0.9871	0.9290	0.9391	0.7093	0.6786	0.5531	0.7655	0.6326	0.6942	0.6722
Spatial	FFD [12]	Xception	22	0.9624	0.8237	0.9803	0.9784	0.9853	0.9306	0.9434	0.7840	0.7435	0.8609	0.8024	0.7029	0.7426	0.7727
Spatial	CORE [47]	Xception	22	0.9638	0.8194	0.9787	0.9803	0.9823	0.9339	0.9431	0.7798	0.7428	0.8475	0.8018	0.7049	0.7341	0.7685
Spatial	UCF [67]	Xception	47	0.9705	0.8399	0.9883	0.9840	0.9896	0.9441	0.9527	0.7793	0.7527	0.8241	0.8074	0.7191	0.7594	0.7737
Spatial	FFD [12]	MkfaNet-S	20	0.9829	0.8475	0.9916	0.9869	0.9937	0.9524	0.9591	0.8065	0.7679	0.8930	0.8194	0.7258	0.7652	0.7963

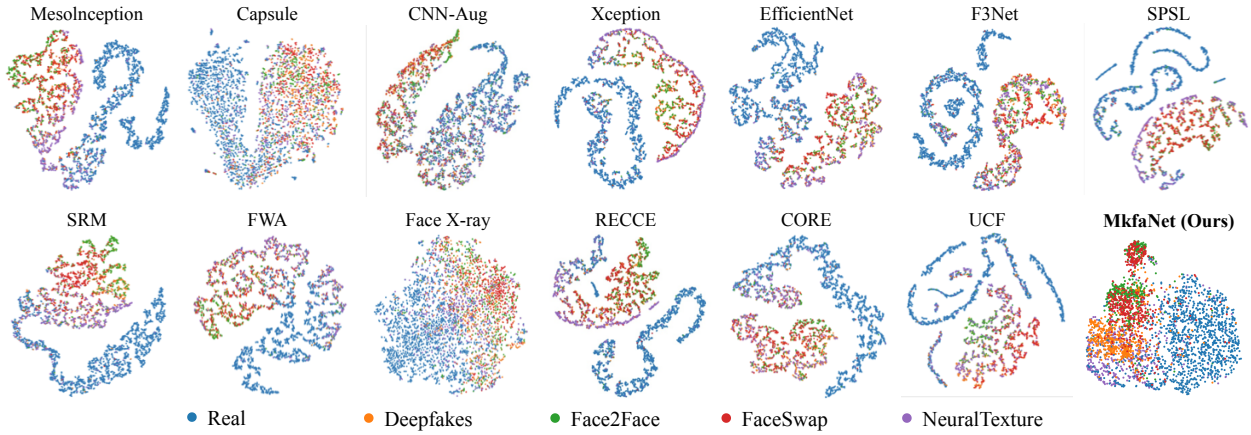


Figure 4. Visualization of latent embedding of detectors with t-SNE [60] on FF++ (c23) according to DeepfakeBench [68].

forms MesoNet [1] and CapsuleNet [46] with similar parameters by 9.33% and 2.87% AUC while outperforming CNN-Aug [63] using only a quarter of the parameters of ResNet-34 [26]. When compared to naive detectors with around 20M parameters, the modern networks (Swin-T [42] and ConvNeXt-T [43]) consistently improve the classical CNNs (ResNet-50 [26], Xception [9], and EfficientNet-B4 [57]), *e.g.*, ConvNeXt-T outperforms ResNet-50 and EfficientNet-B4 by 10.29% and 0.77% AUC on FF-c23, which might attribute to the Metaformer macro design [69] and more parameters. Meanwhile, our proposed MkfaNet-S significantly improves both classical CNNs and modern networks with efficient usage of parameters, *e.g.*, MkfaNet-S yields 94.85% AUC and around 0.25~8.0% performance gains in average comparing to previous backbones. When employing larger backbone encoders with manually-

designed features, FFD [12] with MkfaNet-S significantly outperforms frequency detectors (F3Net [51], SPSL [41], and SRM [45]) and spatial detectors (FWA [39], X-ray [37], and CORE [47]) with Xception and HRNet [56] backbones in the similar parameter scale, while even yielding better results than UCF [67] with a larger Xception backbone.

Cross-domain Evaluations. Then, we evaluate detectors on different datasets without further fine-tuning, which reflects the generalization and robustness of the compared detectors. As shown in Table 1 (right columns), all models suffer performance decreases because of the challenging domain gap. Surprisingly, our proposed MkfaNet variants achieve the best average results and form greater performance gains over existing methods, *e.g.*, Naive detector with MkfaNet-S outperforms Xception and ConvNeXt-T by 1.43% and 1.13% average AUC, indicating that MkfaNet

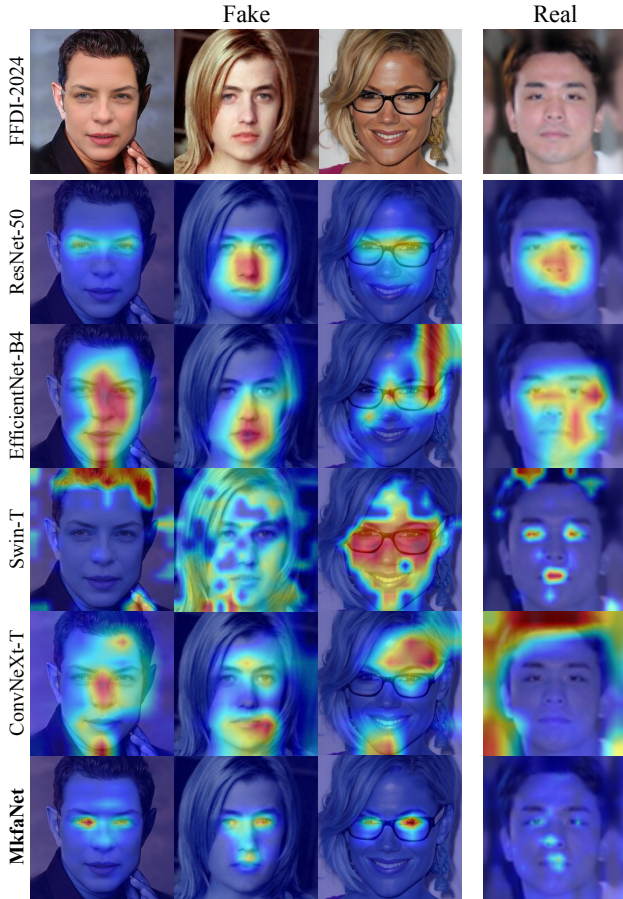


Figure 5. Grad-CAM activation maps [53] of fake and real images in the validation set of FFDI-2024 as cross-domain evaluation. Compare the naive detector with different backbones with ours. As for fake images, classical CNNs like ResNet-50 show robust but coarse localization of human faces, while modern architectures like Swin-T can activate some semantic features. Out MkfaNet not only exhibits precise localization of discriminative organs but also tells the difference between fake and real faces.

might learn more common and robust features. We verify this hypothesis in Sec. 4.3 with visualizations.

4.3. Ablation and Analysis

Ablation studies of network modules. We first ablate the designed modules in MkfaNet with a simplified experimental setting, *i.e.*, training and evaluation on FF-c23 without using ImageNet-1K pre-trained weights. We take ConvNeXt-T [43] as the baseline for MkfaNet, which outperforms the classical bottleneck in ResNet-50 [26] in Table 2. As for the proposed **Multi-kernel Aggregator (MKA)** block, using the **Gating Branch** in Eq. 2 can yield similar performances as ConvNeXt-T with around 10M fewer parameters and using **Multi-DWConv7** \times 7 with dilated ratios in (1, 2, 3) aggregates contextualized patterns and improves the performances. As for the **Multi-**

Block	Module	FF-c23 (AUC)	# Param. (M)
ResNet	Bottleneck	0.8437	25.6
ConvNeXt	DWConv7 \times 7+FFN	0.8856	28.5
MKA	Gating Branch	0.8819	18.5
	+DWConv7 \times 7	0.8932	18.7
	+Multi-DWConv7 \times 7	0.9015	19.0
MFA	DWConv3 \times 3+FFN	0.9093	19.2
	+SE	0.9150	21.5
	+MF	0.9176	19.8

Table 2. Ablation of designed modules on FF-c23. The module without “+” denotes the baseline modules, while those with “+” are added to the baseline (using gray backgrounds).

Frequency Aggregator (MFA) block, adding a Squeeze-and-excitation (SE) module [27] to **DWConv3** \times 3 + **FFN** is equivalent to the EfficientNet block [57], which requires numerous parameters for performance gains. Our proposed **MF** module in Eq. 4 brings better AUC than the SE module while using fewer parameters.

Visualization analysis. We then evaluate the learned features of MkfaNet-S by two visualizations. As shown in Figure 4, the representations of various detectors are visualized by t-SNE [60] on FF++ (c23) dataset with 5000 randomly selected samples following DeepfakeBench, where four forgery types (Deepfakes, Face2Face, FaceSwap, and NeuralTextures) in FF++ are considered. The representations of real and fake samples are more separable in MkfaNet-S than in previous works, while four different forgeries are also discriminative by MkfaNet-S. It indicates that MkfaNet can capture common features rather than over-fitting the training dataset. Meanwhile, we further investigate the spatial features learned by MkfaNet with Grad-CAM [53] visualization in Figure 5. We consider cross-domain evaluation samples from FFDI-2024¹, and compare with various backbone architectures. Figure 5 shows that MkfaNet-S precisely and consistently locates organs to determine fake or real faces, while other backbones sometimes extract irrelevant regions, which might deteriorate the generalization and robustness of forgery detection.

5. Conclusion

In this paper, we introduce MkfaNet, a novel backbone network specifically designed for face forgery detection. It combines two core modules: the Multi-Kernel Aggregator (MKA) and the Multi-Frequency Aggregator (MFA), which effectively enhance the ability to distinguish between real and forged facial features. The MKA module targets

¹The latest Global Multimedia Deepfake Detection competition at <https://www.kaggle.com/competitions/multi-ffdi/data>.

spatial context by adaptively selecting organ-specific features extracted through multiple convolutions to simulate the subtle facial differences between real and fake faces. The MFA module focuses on frequency components, processing different frequency bands by adaptively rebalancing high-frequency and low-frequency features. This innovative approach not only significantly improves the accuracy of forgery detection but also enhances the model's capability to handle complex facial data, making it a powerful tool for combating advanced forgery techniques in the future.

References

- [1] Darius Afchar, Vincent Nozick, Junichi Yamagishi, and Isao Echizen. Mesonet: a compact facial video forgery detection network. In *2018 IEEE international workshop on information forensics and security (WIFS)*, pages 1–7. IEEE, 2018. [2](#), [7](#)
- [2] Weiming Bai, Yufan Liu, Zhipeng Zhang, Bing Li, and Weiming Hu. Aunet: Learning relations between action units for face forgery detection. In *Proceedings of the IEEE/CVF Conference on Computer Vision and Pattern Recognition*, pages 24709–24719, 2023. [2](#), [3](#)
- [3] Sarah Cahlan. How misinformation helped spark an attempted coup in gabon. *The Washington Post*, 13, 2020. [1](#)
- [4] Junyi Cao, Chao Ma, Taiping Yao, Shen Chen, Shouhong Ding, and Xiaokang Yang. End-to-end reconstruction-classification learning for face forgery detection. In *Proceedings of the IEEE/CVF Conference on Computer Vision and Pattern Recognition*, pages 4113–4122, 2022. [2](#)
- [5] Guangyao Chen, Limeng Qiao, Yemin Shi, Peixi Peng, Jia Li, Tiejun Huang, Shiliang Pu, and Yonghong Tian. Learning open set network with discriminative reciprocal points. In *Computer Vision—ECCV 2020: 16th European Conference, Glasgow, UK, August 23–28, 2020, Proceedings, Part III 16*, pages 507–522. Springer, 2020. [2](#)
- [6] Liang Chen, Yong Zhang, Yibing Song, Lingqiao Liu, and Jue Wang. Self-supervised learning of adversarial example: Towards good generalizations for deepfake detection. In *Proceedings of the IEEE/CVF conference on computer vision and pattern recognition*, pages 18710–18719, 2022. [2](#)
- [7] Jongwook Choi, Taehoon Kim, Yonghyun Jeong, Seungryul Baek, and Jongwon Choi. Exploiting style latent flows for generalizing deepfake video detection. In *Proceedings of the IEEE/CVF Conference on Computer Vision and Pattern Recognition*, pages 1133–1143, 2024. [3](#)
- [8] Yunje Choi, Minje Choi, Munyoung Kim, Jung-Woo Ha, Sunghun Kim, and Jaegul Choo. Stargan: Unified generative adversarial networks for multi-domain image-to-image translation. In *Proceedings of the IEEE conference on computer vision and pattern recognition*, pages 8789–8797, 2018. [3](#)
- [9] François Chollet. Xception: Deep learning with depthwise separable convolutions. In *Proceedings of the IEEE conference on computer vision and pattern recognition*, pages 1251–1258, 2017. [2](#), [3](#), [5](#), [7](#)
- [10] Antonia Creswell, Tom White, Vincent Dumoulin, Kai Arulkumaran, Biswa Sengupta, and Anil A Bharath. Generative adversarial networks: An overview. *IEEE signal processing magazine*, 35(1):53–65, 2018. [1](#)
- [11] Florinel-Alin Croitoru, Vlad Hondru, Radu Tudor Ionescu, and Mubarak Shah. Diffusion models in vision: A survey. *IEEE Transactions on Pattern Analysis and Machine Intelligence*, 45(9):10850–10869, 2023. [1](#)
- [12] Hao Dang, Feng Liu, Joel Stehouwer, Xiaoming Liu, and Anil K Jain. On the detection of digital face manipulation. In *Proceedings of the IEEE/CVF Conference on Computer Vision and Pattern Recognition*, 2020. [7](#)
- [13] DeepFakes. www.github.com/deepfakes/faceswap Accessed 2021-04-24. [6](#)
- [14] Liwei Deng, Jiandong Wang, and Zhen Liu. Cascaded network based on efficientnet and transformer for deepfake video detection. *Neural Processing Letters*, 55(6):7057–7076, 2023. [5](#)
- [15] DFD. <https://ai.googleblog.com/2019/09/contributing-data-to-deepfake-detection.html> Accessed 2021-04-24. [6](#), [12](#)
- [16] Brian Dolhansky, Joanna Bitton, Ben Pfau, Jikuo Lu, Russ Howes, Menglin Wang, and Cristian Canton Ferrer. The deepfake detection challenge dataset. *arXiv preprint arXiv:2006.07397*, 2020. [6](#), [12](#)
- [17] Brian Dolhansky, Russ Howes, Ben Pfau, Nicole Baram, and Cristian Canton Ferrer. The deepfake detection challenge (dfdc) preview dataset. *arXiv preprint arXiv:1910.08854*, 2019. [6](#), [12](#)
- [18] Shichao Dong, Jin Wang, Renhe Ji, Jiajun Liang, Haoqiang Fan, and Zheng Ge. Implicit identity leakage: The stumbling block to improving deepfake detection generalization. In *Proceedings of the IEEE/CVF Conference on Computer Vision and Pattern Recognition*, pages 3994–4004, 2023. [3](#)
- [19] FaceSwap. www.github.com/MarekKowalski/FaceSwap Accessed 2021-04-24. [6](#)
- [20] Chao Feng, Ziyang Chen, and Andrew Owens. Self-supervised video forensics by audio-visual anomaly detection. In *Proceedings of the IEEE/CVF Conference on Computer Vision and Pattern Recognition*, pages 10491–10503, 2023. [2](#)
- [21] Shiming Ge, Jia Li, Qiting Ye, and Zhao Luo. Detecting masked faces in the wild with lle-cnns. In *Proceedings of the IEEE conference on computer vision and pattern recognition*, pages 2682–2690, 2017. [2](#)
- [22] Shiming Ge, Shengwei Zhao, Chenyu Li, and Jia Li. Low-resolution face recognition in the wild via selective knowledge distillation. *IEEE Transactions on Image Processing*, 28(4):2051–2062, 2018. [2](#)
- [23] Dimitrios Gerogiannis, Foivos Paraperas Papanitiou, Rolandos Alexandros Potamias, Alexandros Lattas, Stylianos Moschoglou, Stylianos Ploumpis, and Stefanos Zafeiriou. Animateme: 4d facial expressions via diffusion models. *arXiv preprint arXiv:2403.17213*, 2024. [3](#)
- [24] Ian Goodfellow, Jean Pouget-Abadie, Mehdi Mirza, Bing Xu, David Warde-Farley, Sherjil Ozair, Aaron Courville, and Yoshua Bengio. Generative adversarial networks. *Communications of the ACM*, 63(11):139–144, 2020. [3](#)

- [25] Alexandros Haliassos, Konstantinos Vougioukas, Stavros Petridis, and Maja Pantic. Lips don't lie: A generalisable and robust approach to face forgery detection. In *Proceedings of the IEEE/CVF conference on computer vision and pattern recognition*, pages 5039–5049, 2021. 2
- [26] Kaiming He, Xiangyu Zhang, Shaoqing Ren, and Jian Sun. Deep residual learning for image recognition. In *Conference on Computer Vision and Pattern Recognition (CVPR)*, pages 770–778, 2016. 6, 7, 8
- [27] Jie Hu, Li Shen, and Gang Sun. Squeeze-and-excitation networks. In *Conference on Computer Vision and Pattern Recognition (CVPR)*, pages 7132–7141, 2018. 8
- [28] Liming Jiang, Ren Li, Wayne Wu, Chen Qian, and Chen Change Loy. Deepforensics-1.0: A large-scale dataset for real-world face forgery detection. In *Proceedings of the IEEE/CVF conference on computer vision and pattern recognition*, pages 2889–2898, 2020. 2, 6, 12
- [29] Tero Karras, Timo Aila, Samuli Laine, and Jaakko Lehtinen. Progressive growing of gans for improved quality, stability, and variation. *arXiv preprint arXiv:1710.10196*, 2017. 3
- [30] Diederik P. Kingma and Jimmy Ba. Adam: A method for stochastic optimization. 2015. 6, 12
- [31] Diederik P Kingma and Max Welling. Auto-encoding variational bayes. *arXiv preprint arXiv:1312.6114*, 2013. 3
- [32] Diederik P Kingma, Max Welling, et al. An introduction to variational autoencoders. *Foundations and Trends® in Machine Learning*, 12(4):307–392, 2019. 1
- [33] Alex Krizhevsky, Ilya Sutskever, and Geoffrey E. Hinton. Imagenet classification with deep convolutional neural networks. *Communications of the ACM*, 60:84 – 90, 2012. 6, 12
- [34] Binh M Le, Jiwon Kim, Shahroz Tariq, Kristen Moore, Al-sharif Abuadbbba, and Simon S Woo. Sok: Facial deepfake detectors. *arXiv preprint arXiv:2401.04364*, 2024. 2
- [35] Binh M Le and Simon S Woo. Quality-agnostic deepfake detection with intra-model collaborative learning. In *Proceedings of the IEEE/CVF International Conference on Computer Vision*, pages 22378–22389, 2023. 2
- [36] Lingzhi Li, Jianmin Bao, Hao Yang, Dong Chen, and Fang Wen. Faceshifter: Towards high fidelity and occlusion aware face swapping. *arXiv preprint arXiv:1912.13457*, 2019. 3, 12
- [37] Lingzhi Li, Jianmin Bao, Ting Zhang, Hao Yang, Dong Chen, Fang Wen, and Baining Guo. Face x-ray for more general face forgery detection. In *Proceedings of the IEEE/CVF conference on computer vision and pattern recognition*, pages 5001–5010, 2020. 2, 3, 7
- [38] Shikun Li, Xiaobo Xia, Shiming Ge, and Tongliang Liu. Selective-supervised contrastive learning with noisy labels. In *Proceedings of the IEEE/CVF conference on computer vision and pattern recognition*, pages 316–325, 2022. 2
- [39] Yuezun Li and Siwei Lyu. Exposing deepfake videos by detecting face warping artifacts. *arXiv preprint arXiv:1811.00656*, 2018. 7
- [40] Yuezun Li, Xin Yang, Pu Sun, Honggang Qi, and Siwei Lyu. Celeb-df: A new dataset for deepfake forensics. In *Proceedings of the IEEE/CVF Conference on Computer Vision and Pattern Recognition*, 2020. 6, 12
- [41] Honggu Liu, Xiaodan Li, Wenbo Zhou, Yuefeng Chen, Yuan He, Hui Xue, Weiming Zhang, and Nenghai Yu. Spatial-phase shallow learning: rethinking face forgery detection in frequency domain. In *Proceedings of the IEEE/CVF Conference on Computer Vision and Pattern Recognition*, 2021. 7
- [42] Ze Liu, Yutong Lin, Yue Cao, Han Hu, Yixuan Wei, Zheng Zhang, Stephen Lin, and Baining Guo. Swin transformer: Hierarchical vision transformer using shifted windows. In *International Conference on Computer Vision (ICCV)*, 2021. 6, 7
- [43] Zhuang Liu, Hanzi Mao, Chao-Yuan Wu, Christoph Feichtenhofer, Trevor Darrell, and Saining Xie. A convnet for the 2020s. In *Conference on Computer Vision and Pattern Recognition (CVPR)*, pages 11976–11986, 2022. 6, 7, 8, 12
- [44] Ilya Loshchilov and Frank Hutter. Decoupled weight decay regularization. In *International Conference on Learning Representations (ICLR)*, 2019. 6, 12
- [45] Yuchen Luo, Yong Zhang, Junchi Yan, and Wei Liu. Generalizing face forgery detection with high-frequency features. In *Proceedings of the IEEE/CVF conference on computer vision and pattern recognition*, pages 16317–16326, 2021. 2, 7
- [46] Huy H Nguyen, Junichi Yamagishi, and Isao Echizen. Capsule-forensics: Using capsule networks to detect forged images and videos. In *IEEE International Conference on Acoustics, Speech and Signal Processing*, pages 2307–2311. IEEE, 2019. 7
- [47] Yunsheng Ni, Depu Meng, Changqian Yu, Chengbin Quan, Dongchun Ren, and Youjian Zhao. Core: Consistent representation learning for face forgery detection. In *Proceedings of the IEEE/CVF Conference on Computer Vision and Pattern Recognition Workshop*, pages 12–21, 2022. 7
- [48] Yuval Nirkin, Yosi Keller, and Tal Hassner. Fsgan: Subject agnostic face swapping and reenactment. In *Proceedings of the IEEE/CVF international conference on computer vision*, pages 7184–7193, 2019. 3
- [49] Ivan Perov, Daiheng Gao, Nikolay Chervoniy, Kunlin Liu, Sugasa Marangonda, Chris Umé, Mr Dpfks, Carl Shift Facenheim, Luis RP, Jian Jiang, et al. Deepfacelab: Integrated, flexible and extensible face-swapping framework. *arXiv preprint arXiv:2005.05535*, 2020. 3
- [50] Jiameng Pu, Neal Mangaokar, Lauren Kelly, Parantapa Bhat-tacharya, Kavya Sundaram, Mobin Javed, Bolun Wang, and Bimal Viswanath. Deepfake videos in the wild: Analysis and detection. In *Proceedings of the Web Conference 2021*, pages 981–992, 2021. 2
- [51] Yuyang Qian, Guojun Yin, Lu Sheng, Zixuan Chen, and Jing Shao. Thinking in frequency: Face forgery detection by mining frequency-aware clues. In *European conference on computer vision*, pages 86–103. Springer, 2020. 2, 7
- [52] Andreas Rossler, Davide Cozzolino, Luisa Verdoliva, Christian Riess, Justus Thies, and Matthias Nießner. Faceforensics++: Learning to detect manipulated facial images. In *Proceedings of the IEEE/CVF international conference on computer vision*, pages 1–11, 2019. 2, 3, 6, 7, 12
- [53] Ramprasaath R Selvaraju, Michael Cogswell, Abhishek Das, Ramakrishna Vedantam, Devi Parikh, and Dhruv Batra.

- Grad-cam: Visual explanations from deep networks via gradient-based localization. In *Conference on Computer Vision and Pattern Recognition (CVPR)*, pages 618–626, 2017. **8**
- [54] Zehua Sheng, Zhu Yu, Xiongwei Liu, Si-Yuan Cao, Yuqi Liu, Hui-Liang Shen, and Huaqi Zhang. Structure aggregation for cross-spectral stereo image guided denoising. In *Proceedings of the IEEE/CVF Conference on Computer Vision and Pattern Recognition*, pages 13997–14006, 2023. **2**
- [55] Kaede Shiohara and Toshihiko Yamasaki. Detecting deepfakes with self-blended images. In *Proceedings of the IEEE/CVF Conference on Computer Vision and Pattern Recognition*, pages 18720–18729, 2022. **2**
- [56] Ke Sun, Bin Xiao, Dong Liu, and Jingdong Wang. Deep high-resolution representation learning for human pose estimation. In *Conference on Computer Vision and Pattern Recognition (CVPR)*, pages 5693–5703, 2019. **7**
- [57] Mingxing Tan and Quoc Le. Efficientnet: Rethinking model scaling for convolutional neural networks. In *International conference on machine learning*, pages 6105–6114. PMLR, 2019. **2, 3, 5, 6, 7, 8**
- [58] Justus Thies, Michael Zollhöfer, and Matthias Nießner. Deferred neural rendering: Image synthesis using neural textures. *Acm Transactions on Graphics (TOG)*, 38(4):1–12, 2019. **3, 6**
- [59] Justus Thies, Michael Zollhofer, Marc Stamminger, Christian Theobalt, and Matthias Nießner. Face2face: Real-time face capture and reenactment of rgb videos. In *Proceedings of the IEEE conference on computer vision and pattern recognition*, pages 2387–2395, 2016. **3, 6**
- [60] Laurens Van der Maaten and Geoffrey Hinton. Visualizing data using t-sne. *Journal of Machine Learning Research*, 2008. **7, 8**
- [61] Jane Wakefield. Deepfake presidents used in russia-ukraine war. <https://www.bbc.com/news/technology-60780142>. 2022. **1**
- [62] Chengrui Wang and Weihong Deng. Representative forgery mining for fake face detection. In *Proceedings of the IEEE/CVF conference on computer vision and pattern recognition*, pages 14923–14932, 2021. **2**
- [63] Sheng-Yu Wang, Oliver Wang, Richard Zhang, Andrew Owens, and Alexei A Efros. Cnn-generated images are surprisingly easy to spot... for now. In *Proceedings of the IEEE/CVF Conference on Computer Vision and Pattern Recognition*, pages 8695–8704, 2020. **7**
- [64] Yuan Wang, Kun Yu, Chen Chen, Xiyuan Hu, and Silong Peng. Dynamic graph learning with content-guided spatial-frequency relation reasoning for deepfake detection. In *Proceedings of the IEEE/CVF Conference on Computer Vision and Pattern Recognition*, pages 7278–7287, 2023. **2, 5**
- [65] Zhendong Wang, Jianmin Bao, Wengang Zhou, Weilun Wang, and Houqiang Li. Altfreezing for more general video face forgery detection. In *Proceedings of the IEEE/CVF conference on computer vision and pattern recognition*, pages 4129–4138, 2023. **3**
- [66] Simon Woo et al. Add: Frequency attention and multi-view based knowledge distillation to detect low-quality compressed deepfake images. In *Proceedings of the AAAI Conference on Artificial Intelligence*, volume 36, pages 122–130, 2022. **2**
- [67] Zhiyuan Yan, Yong Zhang, Yanbo Fan, and Baoyuan Wu. Ucf: Uncovering common features for generalizable deepfake detection. *arXiv preprint arXiv:2304.13949*, 2023. **7**
- [68] Zhiyuan Yan, Yong Zhang, Xinhang Yuan, Siwei Lyu, and Baoyuan Wu. Deepfakebench: A comprehensive benchmark of deepfake detection. *arXiv preprint arXiv:2307.01426*, 2023. **2, 3, 6, 7, 12**
- [69] Weihao Yu, Chenyang Si, Pan Zhou, Mi Luo, Yichen Zhou, Jiashi Feng, Shuicheng Yan, and Xinchao Wang. Metaformer baselines for vision. *IEEE Transactions on Pattern Analysis and Machine Intelligence*, 46:896–912, 2024. **7**
- [70] Hanqing Zhao, Wenbo Zhou, Dongdong Chen, Tianyi Wei, Weiming Zhang, and Nenghai Yu. Multi-attentional deepfake detection. In *Proceedings of the IEEE/CVF conference on computer vision and pattern recognition*, pages 2185–2194, 2021. **2, 3, 5**
- [71] Tianchen Zhao, Xiang Xu, Mingze Xu, Hui Ding, Yuanjun Xiong, and Wei Xia. Learning self-consistency for deepfake detection. In *Proceedings of the IEEE/CVF international conference on computer vision*, pages 15023–15033, 2021. **2**
- [72] Wenliang Zhao, Yongming Rao, Weikang Shi, Zuyan Liu, Jie Zhou, and Jiwen Lu. Diffswap: High-fidelity and controllable face swapping via 3d-aware masked diffusion. In *Proceedings of the IEEE/CVF Conference on Computer Vision and Pattern Recognition*, pages 8568–8577, 2023. **3**
- [73] Yifan Zhao, Ke Yan, Feiyue Huang, and Jia Li. Graph-based high-order relation discovery for fine-grained recognition. In *Proceedings of the IEEE/CVF conference on computer vision and pattern recognition*, pages 15079–15088, 2021. **2**
- [74] Yinglin Zheng, Jianmin Bao, Dong Chen, Ming Zeng, and Fang Wen. Exploring temporal coherence for more general video face forgery detection. In *Proceedings of the IEEE/CVF international conference on computer vision*, pages 15044–15054, 2021. **3**

Appendix

The appendix section provides details of the MkfaNet network and experiments.

A. Implementation Details

A.1. Network Configurations

We provide detailed architecture configurations of MkfaNet variants in Table A1, where we scale the embedding dimensions and the number of blocks for each stage: (1) MkfaNet-Tiny with embedding dimensions of $\{32, 64, 128, 256\}$ is designed for lightweight deepfake detection scenarios, exhibiting competitive parameter numbers around 5M parameters; (2) MkfaNet-Small utilizes embedding dimensions of $\{64, 128, 320, 512\}$ in comparison to other prevailing modern architectures [43] around 25M parameters.

Table A1. Architecture configurations of MkfaNet variants.

Stage	Output Size	Layer Settings	MkfaNet	
			Tiny	Small
S1	$\frac{H \times W}{4 \times 4}$	Stem	Conv _{3×3} , stride 2, C/2	
		Embed. Dim.	32	64
		# Moga Block	3	2
		MLP Ratio	8	
S2	$\frac{H \times W}{8 \times 8}$	Stem	Conv _{3×3} , stride 2	
		Embed. Dim.	64	128
		# Moga Block	3	3
		MLP Ratio	8	
S3	$\frac{H \times W}{16 \times 16}$	Stem	Conv _{3×3} , stride 2	
		Embed. Dim.	128	320
		# Moga Block	12	10
		MLP Ratio	4	
S4	$\frac{H \times W}{32 \times 32}$	Stem	Conv _{3×3} , stride 2	
		Embed. Dim.	256	512
		# Moga Block	2	2
		MLP Ratio	4	
Parameters (M)			5.2	19.8

A.2. Datasets

As shown in Table A2, we provide detailed information for the used deepfake detection datasets. Among them, FaceForensics++ (FF++) [52] can be divided into five subsets for training and within-domain evaluations, including FF-DF, FF-F2F, FF-FS, FF-NT, and FF-all. Each subset corresponds to a combination of deepfake and real videos from YouTube. Other datasets are used for cross-domain evaluation. We follow pre-processing scripts in DeepfakeBench [68] to prepare the training and testing datasets, which incorporates four major steps, including face detection, face cropping, face alignment, and various other pre-

processing operations. All images are aligned, cropped, and resized to 256×256 resolutions.

Table A2. Summary of used deepfake detection datasets.

Dataset	Domain	Real Videos	Fake Videos	Total Videos	Rights Cleared	Total Subjects	Synthesis Methods
FF++ [52]	Within	1000	4000	5000	NO	N/A	4
FaceShifter [36]	Cross	1000	1000	2000	NO	N/A	1
DFD [15]	Cross	363	3000	3363	YES	28	5
DFDC-P [17]	Cross	1131	4119	5250	YES	66	2
DFDC [16]	Cross	23,654	104,500	128,154	YES	960	8
CelebDF-v1 [40]	Cross	408	795	1203	NO	N/A	1
CelebDF-v2 [40]	Cross	590	5639	6229	NO	59	1
DF-1.0 [28]	Cross	50,000	10,000	60,000	YES	100	1

A.3. Experimental Settings

As for training settings, we utilize Adam optimizer [30] with a basic learning rate of 2×10^{-4} , a batch size of 32 by default. For the naive detectors with modern backbones (e.g., ConvNeXt-T [43]), we utilize AdamW optimizer [44] to fine-tune detectors with the learning rate of 5×10^{-4} and the batch size of 256 according to their official settings on ImageNet-1K [33]. As initializing the parameters with pre-training provides better performance, we also conduct 300-epoch pre-training on ImageNet-1K for MkfaNet-T/S, as shown in Table A3. As for evaluation protocols, we consider the average Area Under the Curve (AUC) over three runs as our primary metric. Furthermore, it is important to note that the validation set is not utilized in our experiments.

Table A3. Hyper-parameters and training recipes for ImageNet-1K of Swin-T, ConvNeXt-T, and our proposed MkfaNet-T/S.

Configuration	Swin Tiny	ConvNeXt Tiny	MkfaNet Tiny/Small
Input resolution	224 ²	224 ²	224 ²
Epochs	300	300	300
Batch size	1024	4096	4096
Optimizer	AdamW	AdamW	AdamW
AdamW (β_1, β_2)	0.9, 0.999	0.9, 0.999	0.9, 0.999
Learning rate	0.001	0.004	0.004
Learning rate decay	Cosine	Cosine	Cosine
Weight decay	0.05	0.05	0.04/0.05
Warmup epochs	20	20	20
Label smoothing ϵ	0.1	0.1	0.1
Stochastic Depth	✓	✓	✓
Rand Augment	9/0.5	9/0.5	9/0.5
Repeated Augment	✓	✗	✗
Mixup α	0.8	0.8	0.1/0.8
CutMix α	1.0	1.0	1.0
Erasing prob.	0.25	0.25	✗/0.25
ColorJitter	✗	✗	✗
Gradient Clipping	✓	✗	✗
EMA decay	✓	✓	✓
Test crop ratio	0.875	0.875	0.90